

# Fatigue life prediction of turbine blades based on a modified equivalent strain model<sup>†</sup>

Jie Zhou, Hong-Zhong Huang\* and Zhaochun Peng

Center for System Reliability and Safety, University of Electronic Science and Technology of China, Chengdu, Sichuan, 611731, China

(Manuscript Received January 7, 2017; Revised April 4, 2017; Accepted May 23, 2017)

## Abstract

Mean stress is known to exert significant effects on fatigue life prediction. Although numerous adjustments have been developed to explain the influence of mean stress, only a few of such adjustments account for mean stress sensitivity. The Smith-Watson-Topper (SWT) model is one of the most widely used models that can provide satisfactory predictions. It is regarded as a case of a Walker model when the material parameter  $\gamma = 0.5$ . The Walker equation considers the mean stress effect and sensitivity, and it can generate accurate predictions in many fatigue programs. In this work, a modified model that accounts for the mean stress effect and sensitivity is proposed to estimate fatigue life. Several sets of experimental data are used to validate the applicability of the proposed model. The proposed model is also compared with the SWT model and the Morrow model. Results show that the proposed model yields more accurate predictions than the other models. The proposed model is applied to predict the fatigue life of a low-pressure turbine blade.

**Keywords:** Fatigue life; Mean stress; Life prediction; Turbine blade; Finite element analysis

## 1. Introduction

Fatigue failure under cyclic loading is a crack initiation and propagation process. It is also a result of damage accumulation or material performance degeneration [1-5]. Fatigue life prediction provides an effective means to avoid major accidents or disasters before failure. Symmetric cyclic loadings without mean stress are typically used in laboratory loading conditions, whereas such fatigue loads are rarely found in practical engineering applications. Various methods have been developed to predict fatigue life without considering mean stress. However, most mechanical components or structures frequently undergo non-symmetrical fatigue loadings. Therefore, the effect of mean stress should be considered to increase the prediction accuracy of fatigue life.

The stress-life ( $S-N$ ) or strain-life ( $\epsilon-N$ ) curves are typically obtained from experiments under symmetric cyclic loading conditions, where mean stress is equal to zero. Mean stress exerts significant effects on fatigue evolution behavior; hence, it should be considered in fatigue life prediction. Haigh indicated that the mean stress effect in the fatigue process is typically presented as a function of stress amplitude versus mean stress, where the load amplitude of the endurance limit decreases with mean stress in a special cyclic loading [6]. These cyclic loading stress relations of structures are described in Table 1.

Table 1. Relationship of cyclic loadings.

	Parameter
Stress ratio $R$	$R = \sigma_{\min} / \sigma_{\max}$
Stress amplitude $\sigma_a$	$\sigma_a = (\sigma_{\max} - \sigma_{\min}) / 2 = \sigma_{\max} (1 - R) / 2$
Mean stress $\sigma_m$	$\sigma_m = (\sigma_{\max} + \sigma_{\min}) / 2 = \sigma_{\max} (1 + R) / 2$

Table 2. Mean stress correction methods.

Researcher	Model
Gerber	$\frac{\sigma_a}{\sigma_{ar}} + \left(\frac{\sigma_m}{\sigma_u}\right)^2 = 1$
Goodman	$\frac{\sigma_a}{\sigma_{ar}} + \frac{\sigma_m}{\sigma_u} = 1$
Soderberg	$\frac{\sigma_a}{\sigma_{ar}} + \frac{\sigma_m}{\sigma_y} = 1$
Morrow	$\frac{\sigma_a}{\sigma_{ar}} + \frac{\sigma_m}{\sigma_f} = 1$
Walker	$\sigma_{ar} = \sigma_{\max}^{1-\gamma} \sigma_a^\gamma = \sigma_{\max} \left(\frac{1-R}{2}\right)^\gamma = \sigma_a \left(\frac{2}{1-R}\right)^\gamma$
SWT	$\sigma_{ar} = \sqrt{\sigma_{\max} \sigma_a} = \sigma_{\max} \sqrt{\frac{1-R}{2}} = \sigma_a \sqrt{\frac{2}{1-R}}$

To date, a reasonable number of mean stress correction methods and theories on fatigue behavior have been proposed through the development of empirical formulations for differ-

\*Corresponding author. Tel.: +86 28 6183 1252

E-mail address: hzhuang@uestc.edu.cn

<sup>†</sup>Recommended by Associate Editor Yang Zheng

© KSME & Springer 2017

ent metallic materials (Table 2); examples of these methods and theories include the Gerber, Goodman, Soderberg, Morrow, Walker, and Smith-Watson-Topper (SWT) models [7].

The mean stress effect evidently varies for different materials because it depends on the mechanical properties of materials. The connotation of mean stress or sensitivity on material fatigue behavior is critical for accurate life estimation. Several models that account for the mean stress effect or sensitivity have been proposed to estimate fatigue life. Lorenzo et al. [8] introduced a new approach to predict fatigue life behavior under mean stress conditions. Nihei et al. [9] developed several damage parameters to describe mean stress in various steel and aluminum alloy materials. Wehner et al. [10] investigated the effects of mean stress on the cyclic deformation and fatigue life of hardened carbon steel. Ince et al. [7] proposed a modification of the Morrow and SWT models to predict fatigue life. Nieslony et al. [11] used a constant stress ratio  $S$ - $N$  curve approach to account for the mean stress effect on fatigue strength. Lv et al. [12] proposed a strain-life model that considered sensitivity to mean stress in materials by incorporating the parameters of the Walker and SWT models. Zhu et al. [13] introduced two mean stress correction factors into an energy-based model for fatigue life prediction.

In Refs. [14, 15], the Walker model demonstrated considerable advantages relative to other models; in this model, an adjustable parameter  $\gamma$  is used to fit different scenarios and form a single trend curve instead of a family of curves. The magnitude of  $\gamma$  is an adjustable constant associated with material properties. It provides a good correction and sensitivity of mean stress in relation to most metallic materials. Parameter  $\gamma$  can be obtained from experiments or fatigue properties in similar materials, such as yield strength, ultimate strength, and fracture limit. The SWT model may be a good choice in practical engineering applications because of the additional effort required to calculate the value of  $\gamma$ .

Among the aforementioned models in Refs. [8-16], the Gerber model cannot consider the effects of compressive stress or tensile stress, and in most cases, compressive stress tends to increase fatigue life, whereas tensile stress decreases it; the Goodman model is extremely inaccurate; the Morrow model cannot be used for aluminum alloys unless the real fracture strength is adopted; the SWT model is more accurate than the other models and is a special case of the Walker model when  $\gamma = 0.5$ ; the Walker model has a material-dependent parameter that can be used to calibrate the relationship among various groups of materials with different cyclic loadings, and the value of  $\gamma$  for some materials can be found in the material handbook [17].

Several conclusions of the presented mean stress effect models are as follows [11].

(1) Some models are proposed based on monotonic tensile tests with constant material properties, such as the Gerber, Goodman, and Soderberg models. These models provide simple modifications using the static properties of materials that are easily obtained. Moreover, they can only justify a few

parts of the properties by using certain static properties, such as fatigue limit, but they disregard changes in material properties (e.g., strength degradation, cyclic hardening, cyclic softening) during fatigue loading. In addition, these models do not consider fatigue behavior and mean stress sensitivity.

(2) A few models, such as the Walker and Kwofie models, which use material-dependent parameters to fit different materials, can describe the realistic performance of materials [18]. These models make accurate fatigue life predictions and can describe material performance. However, different materials show varying performances, and additional efforts are required to determine the values of material-dependent parameters.

For the previously discussed models or theories, nearly all lack a direct formula that correlates the number of cycles with failure and sensitivities to the material. Mean stress sensitivity with various cyclic loadings in fatigue behavior can be observed or detected, but these models disregard the effects. They only allow a simple modification based on statistical data to assess fatigue life. Therefore, material property sensitivities with mean stress should be considered.

Masson [19] established the relationship between fatigue life and total strain without distinguishing whether a given strain is elastic or plastic. The Masson model presents the endurance-limit strain correctly, and it has been utilized extensively in engineering applications. Therefore, a practical method is developed to estimate fatigue life by considering the magnitude of  $\gamma$  based on the Masson model. Several sets of experimental data are used to validate the proposed model, which is also applied to the life prediction of a turbine blade.

## 2. Strain-based life prediction methods

The purpose of fatigue life prediction is to establish an accurate model with good prediction performance [20-30]. Several criteria have been developed to predict fatigue life, and they include stress-based, strain-based, energy-based, and other fracture mechanic approaches [31-33]. Among these methods, strain-based approaches are predominantly used to characterize fatigue life.

Under High cycle fatigue (HCF) regimes, the dominant factor that leads to failure is elastic strain, whereas plastic strain is negligible. The stress-life relationship can be described by the Basquin equation, which is given as

$$\sigma_a = \sigma_f' (2N_f)^b. \quad (1)$$

In accordance with Hooke's law, elastic strain can be written as

$$\frac{\Delta \varepsilon_e}{2} = \frac{\sigma_a}{E} = \frac{\sigma_f'}{E} (2N_f)^b, \quad (2)$$

where  $\sigma_a$  is the stress amplitude,  $\sigma_f'$  is the fatigue strength coefficient,  $b$  is the fatigue strength exponent,  $N_f$  is the

number of cycles to failure,  $\Delta\varepsilon_e$  is the elastic strain amplitude, and  $E$  is the elastic modulus.

Under Low cycle fatigue (LCF) regimes, the dominant factor is plastic strain, whereas elastic strain can be disregarded. The strain-life relationship can be written as

$$\frac{\Delta\varepsilon_p}{2} = \varepsilon_f'(2N_f)^c, \tag{3}$$

where  $\Delta\varepsilon_p$  is the plastic strain amplitude,  $\varepsilon_f'$  is the fatigue ductility coefficient, and  $c$  is the fatigue ductility exponent.

In general, the structure components produce both elastic and plastic strains under service conditions. The only difference is that elastic strain can be recovered. The total strain comprises both elastic and plastic strains, which are given by the Manson-Coffin equation and written as

$$\varepsilon_a = \frac{\Delta\varepsilon}{2} = \frac{\Delta\varepsilon_e}{2} + \frac{\Delta\varepsilon_p}{2} = \frac{\sigma_f'}{E}(2N_f)^b + \varepsilon_f'(2N_f)^c, \tag{4}$$

where  $\varepsilon_a$  is the local strain amplitude.

This relation exhibits certain shortcomings when the components are subjected to load spectra with non-mean stress; thus, it may lead to inaccurate results for life predictions under HCF [34].

Morrow et al. [35] suggested that mean stress exerts greater impact on long life regions than on short life regions. The Morrow model can consider elastic strain, which is given by

$$\varepsilon_a = \frac{\sigma_f' - \sigma_m}{E}(2N_f)^b + \varepsilon_f'(2N_f)^c. \tag{5}$$

The Manson-Coffin equation with SWT modification can account for non-mean stress, and it can be expressed as

$$\varepsilon_a \sigma_{\max} = \frac{(\sigma_f')^2}{E}(2N_f)^{2b} + \varepsilon_f' \sigma_f'(2N_f)^{b+c}. \tag{6}$$

In addition, Masson proposed a formulation [19] to model fatigue life and strain, as shown in Eq. (7). The theory suggests the existence of a strain around the endurance limit, at which point fatigue life is essentially infinite. This relation is given as

$$N_f = A(\Delta\varepsilon - \Delta\varepsilon_e)^\alpha, \tag{7}$$

where  $\Delta\varepsilon_e$  is the endurance-limit strain; and  $A$  and  $\alpha$  are material constants that can be expressed by ductility and ultimate strength, respectively. Although the physical definition of these parameters is not provided, they can be obtained from experimental analysis and then used in Eq. (7).  $\Delta\varepsilon_e$  can evidently be ignored if the value of  $\Delta\varepsilon$  is large under LCF. In this case, Eq. (7) will coincide with the plastic strain in Eq. (3).

In general, some metals (such as aluminum and copper) are believed to have no endurance limit, as verified with experimental data. When the stress amplitude becomes lower than a critical value or the number of loading cycles becomes greater than  $5 \times 10^7$ , the fatigue-life curve will follow a horizontal line. When the stress amplitude becomes lower than a critical value or the number of loading cycles becomes greater than  $5 \times 10^9$ , the test specimen will not fail [36]. Furthermore, the endurance limit can be expressed as  $\sigma_\infty$  (endurance-limit stress) or  $\Delta\varepsilon_c$ . If the cyclic loading amplitude or strain value is lower than  $\sigma_\infty$  or  $\Delta\varepsilon_c$ , then fatigue life moves toward infinity.

The most widely used model to describe fatigue life is the Basquin equation; however, it disregards the influence of endurance-limit-stress, and using it to satisfy HCF is difficult. Weibull proposed a stress-life formula [37] shown as

$$N_f = C_f(\sigma_a - \sigma_\infty)^\beta, \tag{8}$$

where  $C_f$  and  $\beta$  are the material constants and  $\beta < 0$ . Eq. (8) cannot present the mean stress effect, and it only satisfies the fatigue life curve under certain conditions.

Eqs. (7) and (8) can reflect the relationship between fatigue life and stress or strain, but the mean stress effect and sensitivity are not considered. The definition of the material and how its value is obtained are given in Eq. (9) [37]:

$$\begin{cases} A = \varepsilon_f'^2 \\ \Delta\varepsilon_c = \frac{2\sigma_{-1}}{E} - \frac{\varepsilon_f'}{10^{3.5}} \\ \alpha = -2 \end{cases} \tag{9}$$

The assumption in Eq. (9) shows that the fatigue ductility coefficient  $\varepsilon_f'$  is equal to the real fatigue ductility coefficient  $\varepsilon_f$ . However, the values of  $\varepsilon_f$  and  $\varepsilon_f'$  are not always equivalent, and other considerations are required for the problems [38, 39].

### 3. Proposed model

The Walker model is a popular theory for modifying mean stress using the adjustable parameter  $\gamma$ . Hence, the Walker exponent  $\gamma$  is used to modify Eq. (7) by accounting for mean stress.

$$N_f = A_0(\Delta\varepsilon_{eq} - \Delta\varepsilon_0)^{\alpha_0}, \tag{10}$$

where  $\Delta\varepsilon_{eq}$  is the equivalent strain,  $\Delta\varepsilon_0$  is the equivalent strain limit, and  $A_0$  and  $\alpha_0$  are material constants.

In the elastic range, the relation between strain and stress can be expressed as

$$\Delta\varepsilon = \frac{\sigma}{E}. \tag{11}$$

Table 3. Material properties of GH4133.

Temperature $T$ (°C)	Elasticity modulus $E$ (GPa)	Poisson's ratio $\mu$	Yielding stress $\sigma_{0.2}$ (MPa)	Strength limit $\sigma_b$ (MPa)	Reduction of area $\varphi$ (%)	Coefficient of linear expansion $\alpha$ ( $\times 10^{-6}$ / °C)	Density $\rho$ (kg/m <sup>3</sup> )
20	223	0.36	878	1221	31	12.0	8210
400	203	0.35	716	1079	31	13.9	
500	197	0.37	716	1055	29	14.6	
600	190	0.35	692	1030	29	15.0	
700	183	0.35	667	962	26	15.8	
800	176	0.39	530	638	17	16.6	

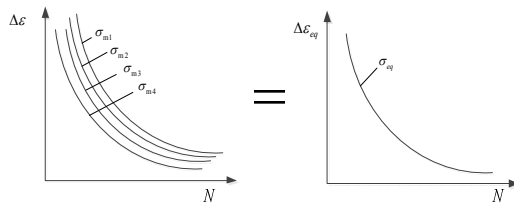


Fig. 1. The equivalent strain-life curve.

Similarly, the equivalent local strain  $\Delta\epsilon_{eq}$  can be expressed as [40]

$$\Delta\epsilon_{eq} = \frac{\sigma_{eq}}{E} = \frac{\sigma_{max}^{1-\gamma} (2\sigma_a)^\gamma}{E} = (2\epsilon_a)^\gamma \left(\frac{\sigma_{max}}{E}\right)^{1-\gamma} \quad (12)$$

Eq. (12) shows that the total strain satisfies Hooke's law if the elastic strain is a dominant factor of fatigue failure. To consider elastic and plastic strains, a compensation factor  $\lambda$  is introduced into Eq. (12) as follows:

$$\Delta\epsilon_{eq} = \lambda \frac{\sigma_{eq}}{E} = \lambda \frac{\sigma_{max}^{1-\gamma} (2\sigma_a)^\gamma}{E} = \lambda (2\epsilon_a)^\gamma \left(\frac{\sigma_{max}}{E}\right)^{1-\gamma} \quad (13)$$

$$\lambda = \begin{cases} 1, & \sigma_{max} \leq \sigma_{0.2} \\ \sigma_{max} / \sigma_{0.2}, & \sigma_{max} > \sigma_{0.2} \end{cases}$$

Thus, a new model for fatigue life prediction can be obtained as

$$N_f = A_0 \left[ \lambda (2\epsilon_a)^\gamma \left(\frac{\sigma_{max}}{E}\right)^{1-\gamma} - \Delta\epsilon_0 \right]^{c_0} \quad (14)$$

In this study, the adjustable parameter  $\gamma$  is incorporated into the Masson model. This model considers the mean stress effect and sensitivity and uses an equivalent strain-life curve instead of a family of strain-life curves (Fig. 1).

#### 4. Life prediction for turbine blades

##### 4.1 Description of turbine blades

Turbine blades are the most at risk components of aero engines with the largest number of whole components. Data on the failures of aircraft components indicate that 70 % of these

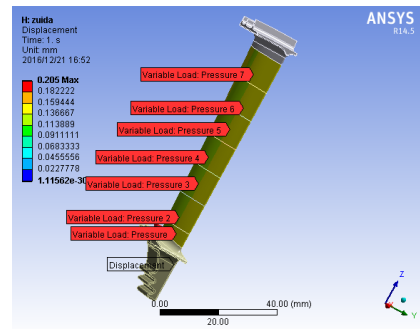


Fig. 2. Aerodynamic forces ( $\omega = 11300$  rpm ).

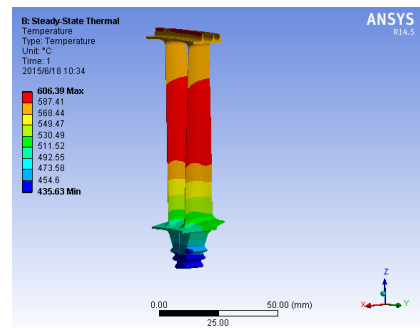


Fig. 3. Thermal stresses ( $\omega = 11300$  rpm ).

failures originate from the blades [41]. Turbine blades work under high temperature and high pressure, and their lives are mainly governed by fatigue. The objective is to predict the fatigue life of a low-pressure turbine blade, which is cast by GH4133 and exhibits high corrosion resistance, good performance under high temperature, and high strength. The material properties of GH4133 [17] are provided in Table 3.

Low-pressure turbine blades endure mechanical and thermal loadings when the aero engine is in service. These blades are subjected to centrifugal forces, thermal stresses, aerodynamic forces, and vibratory stresses. Centrifugal forces, thermal stresses, and aerodynamic forces affect the static analysis of turbine blades, and vibratory stresses can be disregarded. The ANSYS Workbench is typically used as a mathematical tool for Finite element analysis (FEA). The loading spectrum of a low-pressure turbine blade is determined by the flight mission, and it can be divided into three parts according to

Table 4. Loading spectrum of 800 hours.

Working condition	Number of cycles $n_i$	Rotational speed $\omega$ (rpm)
S1	1280	0-11300-0
S2	1940	3500-11300-3500
S3	23330	10000-11300-10000

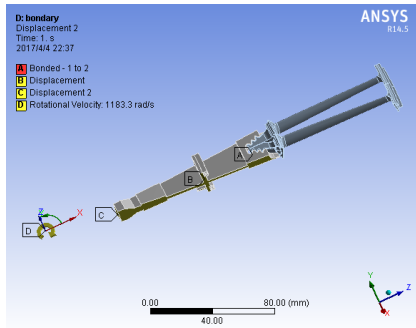


Fig. 4. The boundary conditions of FEA.

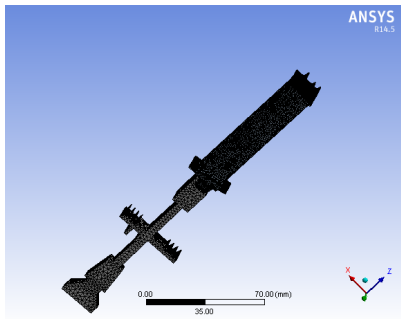


Fig. 5. The meshing grids of FEA.

rotational speed. The loading spectrum of 800 h is shown in Table 4. The thermal stresses and aerodynamic forces are obtained from the experimental data, and the temperature stresses of the turbine blade are loaded onto the 3D model based on the ANSYS Workbench parametric design language for three types of working conditions. The aerodynamic forces are loaded onto the surface of the blades in the ANSYS Workbench, as shown in Figs. 2 and 3. The centrifugal forces are loaded onto the turbine blades by changing rotational velocity.

The low-pressure turbine disc has 47 dovetail joints and 6 bolt holes. When only the dovetail joint is considered and the assembly hole is ignored, only one dovetail joint remains from the disc and the other parts are cut off. The boundary conditions are shown in Fig. 4. The meshing method of the model is automatic classification. The smallest unit of grid control should be used to achieve the computational requirements. The meshing grids of the blade are smaller than those of the disc. In this study, we concentrate only on the grid quality of the blades, as shown in Fig. 5.

We can identify the critical areas of the low-pressure turbine blade under three different working conditions by per-

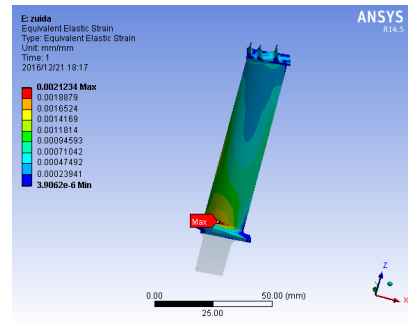
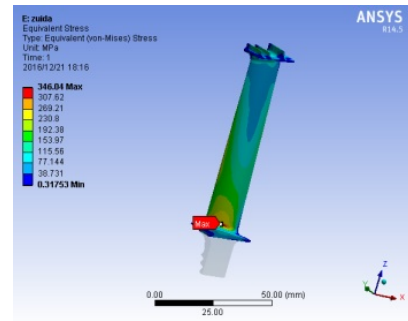


Fig. 6. Stress and strain of circularity transition root ( $\omega = 11300$  rpm).

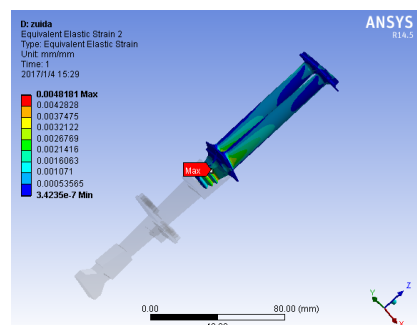
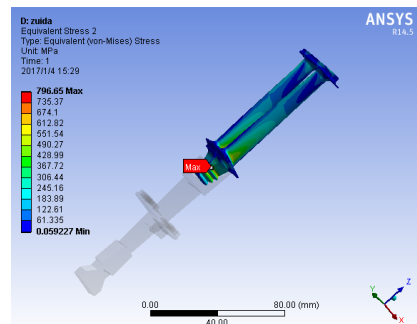


Fig. 7. Stress and strain of fir-tree mortise ( $\omega = 11300$  rpm).

forming FEA. The circularity transition root and the fir-tree mortise are the most critical regions under the same working condition, as shown in Figs. 6 and 7. The results are presented in Table 5.

In accordance with the FEA and other works [42-44], the simulation results show that the maximum stress concentration in the dovetail region occurs in the contact region of the blade root. This condition can be responsible for crack initia-

Table 5. Results of FEA for turbine blade.

Critical area Speed $\omega$ (rpm)	Circularity transition root		Fir-tree mortise	
	Stress (MPa)	Strain (%)	Stress (MPa)	Strain (%)
3500	45.16	0.02779	91.04	0.05458
10000	250.20	0.15358	771.69	0.46466
11300	346.04	0.21234	796.65	0.48181

Table 6. Experimental data under  $T = 250$  °C and  $R = -1$ .

$\varepsilon_a$ (%)	$\sigma_{\max}$ (MPa)	$N_t$	$N_{\text{Proposed}}$	$N_{\text{SWT}}$	$N_{\text{Morrow}}$
0.319	669	30535	15921	46005	68017
0.317	662	18997	16409	49378	71160
0.412	826	7950	6914	7877	13743
0.418	836	6250	6401	7206	12713
0.424	802	11273	7514	7898	11786
0.424	841	9525	6093	6737	11786
0.424	801	4992	7556	7932	11786
0.485	903	5862	3675	3518	6073
0.482	896	4669	3827	3670	6250
0.484	894	5077	3837	3649	6131
0.482	898	5431	3793	3645	6250
0.481	872	5418	4283	4013	6311
0.544	951	3337	2542	2166	3668
0.540	917	3599	2951	2452	3783
0.543	951	3953	2549	2177	3696
0.545	930	5133	2760	2295	3640
0.538	930	4799	2812	2381	3843
0.696	954	2345	1782	1110	1437
0.699	994	1376	1530	990	1416
0.695	991	1684	1558	1012	1444
0.692	1001	1667	1513	997	1466
0.815	1028	944	1111	627	852
0.835	1051	783	999	562	789

tion. The crack will then propagate under fatigue loading and result in a final fracture.

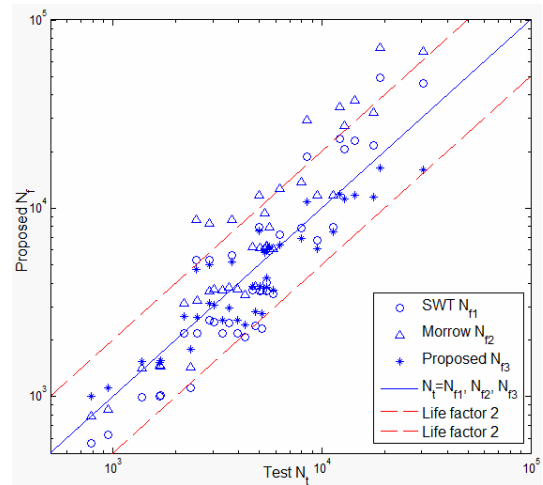
#### 4.2 Experimental data and life prediction

In this section, several sets of experimental data from the material GH4133 [17, 39] (material parameter  $\gamma = 0.55$ ) under different temperatures and stress ratios are used to verify the modified model, as shown in Tables 6-10. The mathematical expression for the proposed model is given in Eq. (15). We present the predicted results for different temperatures in Figs. 8-10 by using Eqs. (5), (6) and (14).

$$\begin{aligned}
 N_{f1} &= 0.1486(\lambda_1 \Delta \varepsilon_{eq} - 0.0022)^{-1.9231}, \quad T = 250^\circ \text{C} \\
 N_{f2} &= 0.1540(\lambda_2 \Delta \varepsilon_{eq} - 0.0027)^{-1.8868}, \quad T = 400^\circ \text{C} \\
 N_{f3} &= 0.1703(\lambda_3 \Delta \varepsilon_{eq} - 0.0029)^{-1.7857}, \quad T = 500^\circ \text{C}.
 \end{aligned} \quad (15)$$

Table 7. Experimental data under  $T = 250$  °C and  $R = 0.44$ .

$\varepsilon_a$ (%)	$\sigma_{\max}$ (MPa)	$N_t$	$N_{\text{Proposed}}$	$N_{\text{SWT}}$	$N_{\text{Morrow}}$
0.3440	777.4	8461	10860	18690	29444
0.3395	743.5	12141	11914	23334	34720
0.3410	755.9	17710	11519	21514	32209
0.3425	741.2	14352	11774	22822	37259
0.3485	748.6	12855	11226	20540	27447
0.4365	863.4	3720	5196	5622	8662
0.4585	806.4	5610	6250	5981	7914
0.4330	886.5	2508	4714	5300	8728
0.4440	864.9	2879	5021	5293	8260
0.4370	841.2	5320	5793	6095	9433
0.5535	932.9	2191	2667	2177	3117
0.5395	904.7	2903	3114	2556	3632
0.5545	935.0	2535	2637	2153	3236
0.5480	961.7	4276	2413	2056	3486
0.5445	905.0	3031	3068	2487	3700

Fig. 8. Predicted life  $N_f$  vs. the test data  $N_t$  under  $T = 250$  °C.

As shown in Figs. 8-10, the life prediction results agree well with the test data with a life factor of  $\pm 2$ . The prediction results of the Morrow and SWT models exhibit a large scatter, whereas the fatigue life estimated by the proposed model is more conservative. To quantify the fatigue life prediction errors of different models, the predicted life deviation is used to indicate accuracy between the logarithmic predicted life and the logarithmic experimental life, as shown in Eq. (16). Then, a standard deviation is calculated as the metric for the life prediction models, as shown in Eq. (17). A small standard deviation means an accurate predicted life. The standard deviations of the fatigue life predictions by the three models are illustrated in Fig. 11.

$$e = \log_{10}(N_f) - \log_{10}(N_t) \quad (16)$$

$$S_e = \sqrt{\frac{\sum_{i=1}^n e_i^2}{n}} \quad (17)$$

Table 8. Experimental data under  $T = 400\text{ }^{\circ}\text{C}$  and  $R = -1$ .

$\varepsilon_a$ (%)	$\sigma_{\max}$ (MPa)	$N_t$	$N_{\text{Proposed}}$	$N_{\text{SWT}}$	$N_{\text{Morrow}}$
0.696	964	1396	1148	937	1071
0.705	894	1071	1482	1086	1026
0.703	893	614	1494	1097	1036
0.702	931	1423	1286	996	1041
0.703	901	916	1446	1073	1036
0.701	915	903	1372	1042	1046
0.699	914	975	1383	1052	1056
0.479	827	4066	3590	3581	4522
0.498	836	4091	3223	3126	3823
0.499	852	3962	2971	2953	3791
0.500	832	2556	3268	3132	3758
0.497	837	4538	3217	3133	3856
0.501	863	2820	2802	2822	3727
0.499	821	2389	3467	3266	3791
0.400	736	9180	8473	8437	10524
0.398	751	7123	7723	8060	10792
0.400	724	12342	9226	8867	10524
0.400	752	8842	7599	7908	10524
0.400	736	7775	8473	8437	10524
0.399	772	5721	6710	7366	10657
0.400	716	8722	9783	9171	10524
0.349	691	12720	13875	15672	21604
0.350	667	13941	14707	17391	21264
0.350	678	15913	14272	16501	21264
0.350	689	13577	13860	15674	21264
0.350	723	12239	12714	13454	21264

Table 9. Experimental data under  $T = 400\text{ }^{\circ}\text{C}$  and  $R = 0$ .

$\varepsilon_a$ (%)	$\sigma_{\max}$ (MPa)	$N_t$	$N_{\text{Proposed}}$	$N_{\text{SWT}}$	$N_{\text{Morrow}}$
0.60	863	1534	2135	1763	1156
0.60	893	1871	1872	1617	1139
0.50	802	4244	3818	3463	2224
0.50	834	3553	3235	3112	2180
0.50	789	3576	4098	3622	2242
0.50	837	4143	3187	3082	2176
0.50	864	4329	2797	2829	2140
0.50	830	4293	3301	3153	2185
0.40	780	7533	6355	7091	5405
0.40	734	7778	8592	8506	5612
0.40	757	6703	7353	7753	5507
0.40	744	8800	8019	8166	5566
0.40	743	4707	8074	8199	5571
0.40	740	6249	8241	8300	5584
0.40	761	6641	7164	7631	5489
0.35	693	12619	13715	15387	10642
0.35	730	13611	11597	13052	10269
0.35	704	11457	13332	14636	10530
0.35	735	10734	11167	12776	10220
0.35	730	12285	11597	13052	10269
0.30	659	20852	21748	30028	24125
0.30	701	19717	19182	24447	22989
0.30	686	19411	20033	26263	23388
0.30	714	18465	18495	23010	22650
0.30	644	13660	22819	32445	24545
0.25	639	30727	38705	62398	70776
0.25	651	26570	36954	58463	69620
0.25	672	44070	34203	52343	67643
0.25	659	29960	35862	56024	68860
0.25	647	45090	37522	59737	70003
0.25	599	41802	45742	78381	74770

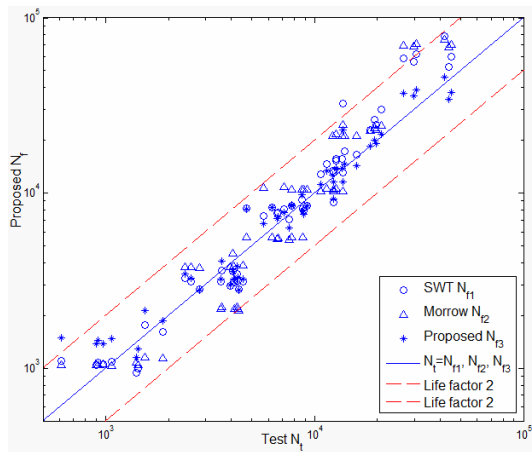


Fig. 9. Predicted life  $N_f$  vs. the test data  $N_t$  under  $T = 400\text{ }^{\circ}\text{C}$ .

As shown in Fig. 11, the standard deviations of the SWT and Morrow models under different temperatures are less than 0.3, whereas those of the proposed model are less than 0.15. The predictability values of the SWT, Morrow, and proposed models are mostly the same, but the life prediction results of the proposed model are closer to the experimental observations than those of the SWT and Morrow models. The proposed method is advantageous because it considers the sensitivity

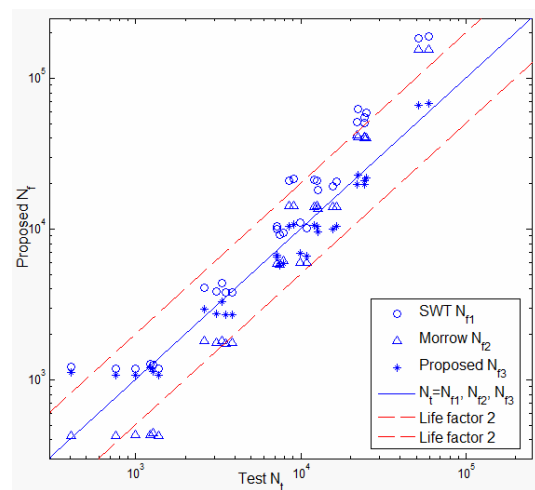


Fig. 10. Predicted life  $N_f$  vs. the test data  $N_t$  under  $T = 500\text{ }^{\circ}\text{C}$ .

Table 10. Experimental data under  $T = 500\text{ }^\circ\text{C}$  and  $R = -1$ .

$\varepsilon_a$ (%)	$\sigma_{\max}$ (MPa)	$N_i$	$N_{\text{Proposed}}$	$N_{\text{SWT}}$	$N_{\text{Morrow}}$
0.703	884	1382	1065	1178	428
0.695	874	1284	1127	1246	446
0.704	882	756	1072	1181	426
0.702	857	1226	1194	1276	430
0.704	871	408	1121	1217	426
0.702	883	993	1072	1186	430
0.500	792	3840	2704	3822	1772
0.498	759	3353	3280	4357	1807
0.498	778	2592	2940	4063	1807
0.501	788	3101	2755	3854	1755
0.502	792	3523	2687	3779	1738
0.401	714	7163	6532	9915	5906
0.398	732	7888	5874	9398	6180
0.400	711	10812	6612	10122	5995
0.402	732	7487	5760	9115	5818
0.401	703	7172	6704	10402	5906
0.400	691	9936	6937	11058	5995
0.350	650	16365	10385	20601	14002
0.350	664	15722	9972	19215	14002
0.349	649	8473	10486	20901	14272
0.349	643	9031	10676	21548	14272
0.351	674	12762	9632	18134	13739
0.349	650	12573	10455	20795	14272
0.350	643	12054	10604	21346	14002
0.301	565	24303	20914	55237	39936
0.300	548	22081	22799	62205	40906
0.301	555	24836	21858	58801	39936
0.300	582	24155	19656	50394	40906
0.299	582	21921	19850	50983	41905
0.251	481	59542	67992	189619	154209
0.251	484	51455	66333	185317	154209

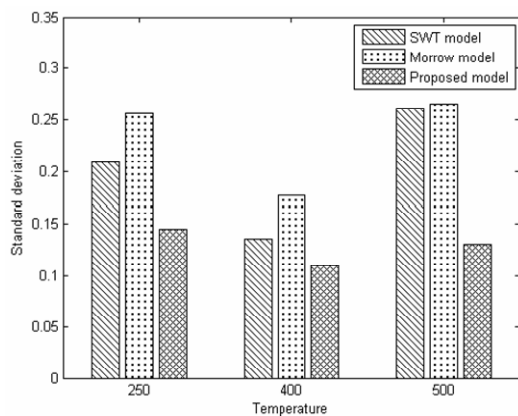


Fig. 11. Standard deviation of fatigue life prediction.

parameter of the Walker equation, which tends to predict a low deviation of fatigue life if the material parameters match well. The prediction accuracy using the proposed model is improved,

Table 11. Life prediction results of proposed model for turbine blade.

	S1	S2	S3
$\omega$ (rpm)	0-11300-0	3500-11300-3500	10000-11300-10000
$n_i$	1280	1940	23330
$\sigma_{\max}$ (MPa)	796.65	796.65	796.65
$\sigma_{\min}$ (MPa)	0	91.04	771.69
$\sigma_a$ (MPa)	398.33	352.81	12.47
$\varepsilon_a$ (%)	0.240905	0.213615	0.008575
$\Delta\varepsilon_{\text{eq}}$ (%)	0.439318	0.411208	0
$\lambda$	1.11	1.11	1.11
$N_f$	16243	21750	$+\infty$

and the model is suitable for life prediction under LCF.

### 4.3 Life prediction of the proposed model for turbine blades

As shown in Table 5, the most critical area of a low-pressure turbine blade is the fir-tree mortise. The temperature of the working conditions is close to  $400\text{ }^\circ\text{C}$ . The life prediction results of the proposed model are shown in Table 11.

The state of S3 can be neglected because the cumulative damage is minimal. In this study, we use a nonlinear fatigue damage model [45] to obtain a cumulative damage of 800 h under different working conditions, as shown in Eq. (18). Thus, the fatigue life of the low-pressure turbine blade can be calculated by Eq. (19).

$$D_{800} = \left(\frac{n_1}{N_{f1}}\right)^{\frac{\ln N_{f2}}{\ln N_{f1}}} + \frac{n_2}{N_{f2}} \tag{18}$$

$$= \left(\frac{1280}{16243}\right)^{\frac{\ln 21750}{\ln 16243}} + \frac{1940}{21750} = 0.1622$$

$$T = 800 \times \frac{1}{D_{800}} = 4932\text{h}. \tag{19}$$

The experimental fatigue life and real fatigue life in service differ considerably, and conducting fatigue experiments under HCF/LCF combined loading or multi-axial tests is difficult due to the complex working conditions of the blades. The presumption is that the failure mode of the blades is HCF/LCF fracture. In such case, experiments with standard specimens may be a good choice. Then, the proposed model can be used in such situation to predict fatigue life. To obtain the real fatigue life of components or structures based on the experimental data, we assume that fatigue life and strength follow the logarithmic normal distribution, and we consider a life factor  $\delta$  on log mean life [46]. The modified fatigue life can be expressed as

$$T_{\text{mod}} = \frac{T}{\delta} = \frac{4932}{2.86} = 1724.5\text{h}. \tag{20}$$

## 5. Conclusions

A modified model that accounts for both the mean stress effect and sensitivity is proposed in this study to predict fatigue life. Several sets of data are used to validate the applicability and accuracy of the proposed model. Two widely used models are also adopted for comparison. In addition, FEA is performed to identify the critical areas of a low-pressure turbine, and the stress and strain of critical areas are obtained using the ANSYS Workbench. The proposed model is also used to predict the fatigue life of a turbine blade by accounting for the mean stress based on a flight mission. The following conclusions are drawn from the obtained results.

(1) The proposed model incorporates the mean stress effect and sensitivity, and it can provide more accurate results than the SWT and Morrow models. However, it cannot be used to predict fatigue life if the mean stress is less than zero.

(2) The material-dependent parameter  $\gamma$  can adjust several strain-life curves under different loadings to a single strain-life curve. It also extends the life prediction range from LCF to HCF, which shows good agreement from  $10^3$  to  $10^6$  with the experimental data.

(3) The FEA results show that the critical regions of the low-pressure turbine blade can be obtained and that the findings can be explored further in future studies.

(4) The proposed model is validated with the experimental data for standard specimens under simple fatigue loading. The equivalent stress/strain and life factor should be considered when the proposed model is used to predict the fatigue life of complex structures or components in practical engineering applications.

## Acknowledgment

This research was supported by the Fundamental Research Funds for the Central Universities under contract numbers ZYGX2014Z010 and SKLMT-KFKT-201601.

## Nomenclature

$\gamma$	: Walker exponent
$\sigma_a$	: Stress amplitude
$\sigma_m$	: Mean stress
$\sigma_{\max}$	: Maximum stress
$\sigma_{\min}$	: Minimum stress
$\sigma_f$	: Fracture strength
$\sigma_u$	: Ultimate tensile strength
$\sigma_y$	: Yield strength
$\sigma'_f$	: Fatigue strength coefficient
$\sigma_{ar}$	: Equivalent fully reversed stress amplitude
$\sigma_\infty$	: Endurance limit stress amplitude
$\sigma_{-1}$	: Fatigue limit stress
$\Delta\sigma_{eq}$	: Local equivalent stress
$\sigma$	: Applied load stress level
$R$	: Stress ratio

$\Delta\varepsilon_a$	: Strain amplitude
$\Delta\varepsilon_e$	: Elastic strain amplitude
$\Delta\varepsilon_p$	: Plastic strain amplitude
$\Delta\varepsilon_c$	: Endurance limit strain
$\Delta\varepsilon_{eq}$	: Local equivalent strain
$\Delta\varepsilon_0$	: Equivalent endurance limit strain
$\varepsilon_f$	: Real fatigue ductility coefficient
$\varepsilon'_f$	: Fatigue ductility coefficient
$C_f$	: Fatigue resistance coefficient
$b$	: Fatigue strength exponent
$c$	: Fatigue ductility exponent
$E$	: Elastic modulus
$N_f$	: Predicted life
$N_i$	: Experimental life
$\lambda$	: Compensation factor
$\delta$	: Life factor
$A_0, \alpha_0$	: Material constant

## References

- [1] W. Peng, Y. F. Li, Y. J. Yang, J. Mi and H. Z. Huang, Bayesian degradation analysis with inverse Gaussian process models under time-varying degradation rates, *IEEE Transactions on Reliability*, 66 (1) (2017) 84-96.
- [2] W. Peng, Y. F. Li, Y. J. Yang, S. P. Zhu and H. Z. Huang, Bivariate analysis of incomplete degradation observations based on inverse Gaussian processes and copulas, *IEEE Transactions on Reliability*, 65 (2) (2016) 624-639.
- [3] W. Peng, Y. F. Li, Y. J. Yang, H. Z. Huang and M. J. Zuo, Inverse Gaussian process models for degradation analysis: A Bayesian perspective, *Reliability Engineering & System Safety*, 130 (2014) 175-189.
- [4] W. Peng, Y. F. Li, J. Mi, L. Yu and H. Z. Huang, Reliability of complex systems under dynamic conditions: A Bayesian multivariate degradation perspective, *Reliability Engineering & System Safety*, 153 (2016) 75-87.
- [5] W. Peng, Y. F. Li, Y. J. Yang, J. Mi and H. Z. Huang, Leveraging degradation testing and condition monitoring for field reliability analysis with time-varying operating missions, *IEEE Transactions on Reliability*, 64 (4) (2015) 1367-1382.
- [6] F. Klubberg, I. Klopfer, C. Broeckmann, R. Berchtold and P. Beiss, Fatigue testing of materials and components under mean load conditions, *Anales de Mecánica de la Fractura*, 1 (2011) 419-424.
- [7] A. Ince and G. Glinka, A modification of Morrow and Smith-Watson-Topper mean stress correction models, *Fatigue & Fracture of Engineering Materials & Structures*, 34 (11) (2011) 854-867.
- [8] F. Lorenzo and C. Laird, A new approach to predicting fatigue life behavior under the action of mean stresses, *Materials Science and Engineering*, 62 (2) (1984) 205-210.
- [9] M. Nihei, P. Heuler, C. Boller and T. Seeger, Evaluation of mean stress effect on fatigue life by use of damage parameters, *International Journal of Fatigue*, 8 (3) (1986) 119-126.
- [10] T. Wehner and A. Fatemi, Effects of mean stress on fatigue

- behavior of a hardened carbon steel, *International Journal of Fatigue*, 13 (3) (1991) 241-248.
- [11] A. Niesłony and M. Böhm, Mean stress effect correction using constant stress ratio S-N curves, *International Journal of Fatigue*, 52 (2013) 49-56.
- [12] Z. Lv, H. Z. Huang, H. K. Wang, H. Gao and F. J. Zuo, Determining the Walker exponent and developing a modified Smith-Watson-Topper parameter model, *Journal of Mechanical Science and Technology*, 30 (3) (2016) 1129-1137.
- [13] S. P. Zhu, Q. Lei, H. Z. Huang, Y. J. Yang and W. Peng, Mean stress effect correction in strain energy-based fatigue life prediction of metals, *International Journal of Damage Mechanics* (2016) DOI: 1056789516651920.
- [14] N. E. Dowling, C. A. Calhoun and A. Arcari, Mean stress effects in stress-life fatigue and the Walker equation, *Fatigue & Fracture of Engineering Materials & Structures*, 32 (3) (2009) 163-179.
- [15] N. E. Dowling, Mean stress effects in stress-life and strain-life fatigue (No. 2004-01-2227), *SAE Technical Paper* (2004).
- [16] S. P. Zhu, Y. J. Yang, H. Z. Huang, Z. Lv and H. K. Wang, A unified criterion for fatigue-creep life prediction of high temperature components, *Proceedings of the IMechE, Part G: Journal of Aerospace Engineering*, 231 (4) (2017) 677-688.
- [17] C. X. Shi, M. G. Yan and Z. Q. Zhu, *China aeronautical materials handbook*, Standards Press of China, Beijing, China (2001).
- [18] S. Kwofie, An exponential stress function for predicting fatigue strength and life due to mean stresses, *International Journal of Fatigue*, 23 (9) (2001) 829-836.
- [19] S. S. Manson, Fatigue: A complex subject—some simple approximations, *Experimental Mechanics*, 5 (7) (1965) 193-226.
- [20] Z. Y. Yu, S. P. Zhu, Q. Liu and Y. Liu, A new energy-critical plane damage parameter for multiaxial fatigue life prediction of turbine blades, *Materials*, 10 (5) (2017) 513.
- [21] H. Z. Huang, H. K. Wang, Y. F. Li, L. Zhang and Z. Liu, Support vector machine based estimation of remaining useful life: current research status and future trends, *Journal of Mechanical Science and Technology*, 29 (1) (2015) 151-163.
- [22] Z. Lv, H. Z. Huang, H. Gao, F. J. Zuo and H. K. Wang, Lifetime prediction for turbine discs based on a modified Walker strain model, *Journal of Mechanical Science and Technology*, 29 (10) (2015) 4143-4152.
- [23] H. Gao, H. Z. Huang, Z. Lv, F. J. Zuo and H. K. Wang, An improved Corten-Dolan's model based on damage and stress state effects, *Journal of Mechanical Science and Technology*, 29 (8) (2015) 3215-3223.
- [24] K. Kim and Y. S. Lee, Dynamic test and fatigue life evaluation of compressor blades, *Journal of Mechanical Science and Technology*, 28 (10) (2014) 4049-4056.
- [25] Y. Kim, K. Lee, H. Li, C. S. Seok, J. M. Koo, S. Y. Kwon and Y. H. Cho, Fatigue life prediction method for contact wire using maximum local stress, *Journal of Mechanical Science and Technology*, 29 (1) (2015) 67-70.
- [26] Z. R. Wu, X. T. Hu, Z. X. Li and Y. D. Song, Prediction of multiaxial fatigue life for notched specimens of titanium alloy TC4, *Journal of Mechanical Science and Technology*, 30 (5) (2016) 1997-2004.
- [27] Y. F. Li, S. P. Zhu, J. Li, W. Peng and H. Z. Huang, Uncertainty analysis in fatigue life prediction of gas turbine blades using Bayesian inference, *International Journal of Turbo & Jet Engines*, 32 (4) (2015) 319-324.
- [28] S. P. Zhu, H. Z. Huang, W. Peng, H. K. Wang and S. Mahadevan, Probabilistic Physics of Failure-based framework for fatigue life prediction of aircraft gas turbine discs under uncertainty, *Reliability Engineering & System Safety*, 146 (2016) 1-12.
- [29] S. P. Zhu, H. Z. Huang, Y. Li, Y. Liu and Y. Yang, Probabilistic modeling of damage accumulation for time-dependent fatigue reliability analysis of railway axle steels, *Proceedings of the IMechE, Part F: Journal of Rail and Rapid Transit*, 229 (1) (2015) 23-33.
- [30] Y. F. Li, Z. Lv, W. Cai, S. P. Zhu and H. Z. Huang, Fatigue life analysis of turbine disks based on load spectra of aero-engines, *International Journal of Turbo & Jet Engines*, 33 (1) (2016) 27-33.
- [31] A. M. Korsunsky, D. Dini, F. P. Dunne and M. J. Walsh, Comparative assessment of dissipated energy and other fatigue criteria, *International Journal of Fatigue*, 29 (9) (2007) 1990-1995.
- [32] J. Schijve, *Fatigue of structures and materials*, Dordrecht: Kluwer Academic (2001).
- [33] S. Kwofie and H. D. Chandler, Low cycle fatigue under tensile mean stresses where cyclic life extension occurs, *International Journal of Fatigue*, 23 (4) (2001) 341-345.
- [34] G. P. Sendecky, Constant life diagrams—a historical review, *International Journal of Fatigue*, 23 (4) (2001) 347-353.
- [35] J. D. Morrow and D. F. Socie, *Review of contemporary approaches to fatigue damage analysis*, Risk and Failure Analysis for Improved Performance and Reliability, Edited by J. J. Burke and V. Weiss, Plenum Publishing Corporation (1980).
- [36] W. Hessler, H. Müller, B. Weiss and H. Schmidt, Fatigue limit of Cu and Al up to  $10^{10}$  loading cycles, *Ultrasonic Fatigue (Proc. AIME)*, New York (1981) 245-263.
- [37] X. L. Zheng, H. Wang, J. H. Tan and X. W. Yi, *Material fatigue theory and engineering application*, Science Press, Beijing, China (2013).
- [38] T. Zhao and Y. Jiang, Fatigue of 7075-T651 aluminum alloy, *International Journal of Fatigue*, 30 (5) (2008) 834-849.
- [39] W. G. Wang, *Research on prediction model for disc LCF life and experiment assessment methodology*, Nanjing University of Aeronautics and Astronautics, Nanjing, China (2006).
- [40] C. E. Jaske, C. E. Feddersen, K. B. Davis and R. C. Rice, *Analysis of Fatigue, Fatigue Crack Propagation and Fracture Data*, Final Report to NASA-Langley Research Center,

NASA Cr-132332 (1973).

- [41] C. Tao, P. Zhong and R. Z. Li, *Failure analysis and prevention for rotor in aero-engine*, National Defence Industry Press, China (2000) 102-163.
- [42] J. Hou, B. J. Wicks and R. A. Antoniou, An investigation of fatigue failures of turbine blades in a gas turbine engine by mechanical analysis, *Engineering Failure Analysis*, 9 (2) (2002) 201-211.
- [43] M. Park, Y. H. Hwang, Y. S. Choi and T. G. Kim, Analysis of a J69-T-25 engine turbine blade fracture, *Engineering Failure Analysis*, 9 (5) (2002) 593-601.
- [44] A. Kermanpur, H. S. Amin, S. Ziaei-Rad, N. Nourbakhshnia and M. Mosaddeghfar, Failure analysis of Ti6Al4V gas turbine compressor blades, *Engineering Failure Analysis*, 15 (8) (2008) 1052-1064.
- [45] D. Ye and Z. Wang, A new approach to low-cycle fatigue damage based on exhaustion of static toughness and dissipation of cyclic plastic strain energy during fatigue, *International Journal of Fatigue*, 23 (8) (2001) 679-687.
- [46] *DEF STAN 00-971*, General Specification for Aircraft Gas Turbine Engines, UK, Ministry of Defense (1987).



**Jie Zhou** is currently a Ph.D. candidate in Mechanical Engineering at the University of Electronic Science and Technology of China. He obtained his B.S. in Mechanical Design, Manufacturing, and Automation from the University of Electronic Science and Technology of China in 2013. His research interests include

fatigue life prediction and fatigue reliability analysis.



**Hong-Zhong Huang** is a Professor of the School of Mechanical, Electronic, and Industrial Engineering at the University of Electronic Science and Technology of China. He has held visiting appointments at several universities in the USA, Canada, and Asia. He obtained his Ph.D. degree in Reliability Engineer-

ing from Shanghai Jiaotong University, China, and he has published 200 journal papers and 5 books in the fields of reliability engineering, optimization design, fuzzy sets theory, and product development.



**Zhaochun Peng** is currently a Ph.D. candidate in Mechanical Engineering at the University of Electronic Science and Technology of China. He obtained his B.S. in Mechanical Design, Manufacturing, and Automation from the University of Electronic Science and Technology of China in 2011. His research

interests include fatigue life prediction and fatigue reliability analysis.